Introducing an Irrigation Scheme to a Regional Climate Model: A Case Study over West Africa

MARC P. MARCELLA AND ELFATIH A. B. ELTAHIR

Massachusetts Institute of Technology, Cambridge, Massachusetts

(Manuscript received 15 February 2013, in final form 7 July 2013)

ABSTRACT

This article presents a new irrigation scheme and biome to the dynamic vegetation model, Integrated Biosphere Simulator (IBIS), coupled to version 3 of the Regional Climate Model (RegCM3-IBIS). The new land cover allows for only the plant functional type (crop) to exist in an irrigated grid cell. Irrigation water (i.e., negative runoff) is applied until the soil root zone reaches relative field capacity. The new scheme allows for irrigation scheduling (i.e., when to apply water) and for the user to determine the crop to be grown. Initial simulations show a large sensitivity of the scheme to soil texture types, how the water is applied, and the climatic conditions over the region. Application of the new scheme is tested over West Africa, specifically Mali and Niger, to simulate the potential irrigation of the Niger River. A realistic representation of irrigation of the Niger River is performed by constraining the land irrigated by the annual flow of the Niger River and the amount of arable land in the region as reported by the Food and Agriculture Organization of the United Nations (FAO). A 30-yr simulation including irrigated cropland is compared to a 30-yr simulation that is identical but with no irrigation of the Niger. Results indicate a significant greening of the irrigated land as evapotranspiration over the crop fields largely increases—mostly via increases in transpiration from plant growth. The increase in the evapotranspiration, or latent heat flux (by 65–150 $W m^{-2}$), causes a significant decrease in the sensible heat flux while surface temperatures cool on average by nearly 5°C. This cooling is felt downwind, where average daily temperatures outside the irrigation are reduced by 0.5°–1.0°C. Likewise, large increases in 2-m specific humidity are experienced across the irrigated cropland (on the order of 5 $g kg^{-1}$) but also extend farther north and east, reflecting the prevailing surface southwesterlies. Changes (decreases) in rainfall are found only over the irrigated lands of west Mali. The decrease in rainfall can be explained by the large surface cooling and collapse of the boundary layer (by approximately 500 m). Both lead to a reduction in the triggering of convection as the convective inhibition, or negative buoyant energy, is never breached. Nevertheless, the new scheme and land cover allows for a novel line of research that can accurately reflect the effects of irrigation on climate and the surrounding environment using a dynamic vegetation model coupled to a regional climate model.

1. Introduction

Over many semiarid regions across the world, the practice of irrigation offers the opportunity to supply water for crop growth that would otherwise be unfeasible. Many modeling studies have investigated the effects of this anthropogenic forcing on regional climate's across the globe (e.g., Segal et al. 1998; Lobell et al. 2009; Marcella and Eltahir 2012). Namely, Pielke et al. (2007) provides a large overview and review of the direct and indirect effects of irrigation on regional climates. However, few, if any, have coupled an irrigation scheme to a dynamic vegetation land surface model, such as the Integrated Biosphere Simulator (IBIS). Doing so provides the unique opportunity to investigate the effects on vegetation competition and environment outside of the irrigated crop region due to climate changes caused by the irrigation.

In this work, the authors first describe a new irrigation scheme and biome added to the land surface model (IBIS) of the Regional Climate Model, version 3 (RegCM3). The performance of the irrigation scheme is then evaluated based on changes to land surface features and fluxes such as soil moisture, evapotranspiration, leaf area index, canopy height, and water requirements. Finally, a case study using the new scheme is performed

Corresponding author address: Marc Pace Marcella, Ralph M. Parsons Laboratory, Dept. of Civil and Environmental Engineering, Building 48-216, Massachusetts Institute of Technology, 77 Massachusetts Avenue, Cambridge, MA 02139.
E-mail: marcpace@mit.edu

DOI: 10.1175/JCLI-D-13-00116.1

over Mali and Niger by adding the irrigation of the Niger River. By comparing a simulation with irrigation to one without, the analysis is completed in determining the effects of potential irrigation on the surface climate of the Sahel in West Africa.

2. Adding an irrigation scheme to IBIS

a. Biome description

In its original formation, IBIS has 16 biomes—15 natural land covers and 1 anthropogenic land cover (cropland) (Foley et al. 1996; Winter and Eltahir 2010). Respectively, there are 13 naturally occurring plant functional types (PFTs) that can occupy the natural biomes and one human-grown plant type, a crop that can live in the cropland biome. The crop plant parameters (phenology thresholds, photosynthesis rates, etc.) are based on the properties of corn and are taken from the work of Kucharik et al. (2000). Over West Africa, the use of corn may not be the most adequate plant type to use, as millet and sorghum are the widespread crops grown. While any PFT can compete in any natural biome, only the crop PFT can exist in a cropland. Following this work, a new anthropogenic biome is added to RegCM3-IBIS: irrigated cropland. The only PFT allowed in the new biome is a crop (for which the physiology and phenology parameters can be specified). Given its anthropogenic characteristics, irrigated cropland (like cropland) will remain an irrigated cropland even when RegCM3-IBIS is run in dynamic vegetation mode; that is, the land cover is considered a static biome. Similarly, the crop PFT is allowed to grow all year with seeds planted in January; however, given its high water needs, over the Sahel and Sahara, crops are largely constrained during nonirrigated periods of the year. In addition, irrigation scheduling (i.e., applying water at certain times of the day, week, month, or year) is also allowed. Here, irrigation is assumed to occur from May–September (at every time step), since this is the growing season of most crops in Mali and Niger (Frenken and Faures 1997).

b. Water application and water balance

Presented in Fig. 1 is a schematic illustrating the principal hydrological components and fluxes for an irrigated cropland. Essentially, the change in storage ΔS, or the soil moisture of a layer, is calculated based on the amount of precipitation P that falls and subsequently infiltrates a given layer, minus that which runs off, runoff R. and that which evaporates from the bare ground and canopy or transpires through plants, evapotranspiration (ET). Therefore, by specifying a set value for the root zone soil moisture, in terms of its relative saturation s_{rz} (volumetric soil moisture divided by porosity), one can calculate the amount of water needed to irrigate (I) a region to a set soil moisture value.

Here, this set soil moisture value s, the relative soil saturation, is assumed to be the relative field capacity, which is the field capacity θ_{fc} divided by the porosity ϕ of a soil layer. A similar approach to modeling irrigation via saturation to field capacity has been carried out by several other studies (Adegoke et al. 2003; Haddeland et al. 2006; Kueppers et al. 2007). Both θ_{fc} and ϕ for the four layers that constitute the root zone (the top 1 m of soil) are given based on the observational soil texture input datasets of IBIS. From these four layers, a weighted (based on the depth of each of the four layers) average root zone relative soil saturation of field capacity is computed. For each time step in which irrigation is active, the root zone is then forced to this relative soil saturation value by adding I or $-R'$ irrigation water (i.e., negative runoff) to the root zone. The negative runoff value is important not only to conserve the water balance of the column but also as a diagnostic to calculate the total water needed for irrigation.

The step by step computations for the irrigation scheme are as follows (please refer to Fig. 1 for a schematic explanation of the required variables and calculated values):

1) Calculate the actual water in the root zone (rz; i.e., the top 1 m) termed root_wat, where θ is the volumetric soil water content, h is the depth of the soil layer, and z the soil layer level:

$$\text{root\_wat} = \sum_{z=0}^{\text{rz}} \theta_z h_z . \tag{1}$$

2) Determine the maximum water that can exist in the root zone (gwmax) where ϕ is the porosity of each soil layer:

$$\text{gwmax} = \sum_{z=0}^{\text{rz}} \phi_z h_z . \tag{2}$$

3) Find the weighted average root zone relative soil saturation at field capacity (rel_fc):

$$\text{rel\_fc} = \sum_{z=0}^{\text{rz}} \frac{\theta_{\text{fc}_z}}{\phi_z}. \tag{3}$$

4) Compute the fraction of water already in the root zone (frac_wat), which is the relative soil saturation of the root zone:

$$\text{frac\_wat} = \frac{\text{root\_wat}}{\text{gwmax}}. \tag{4}$$

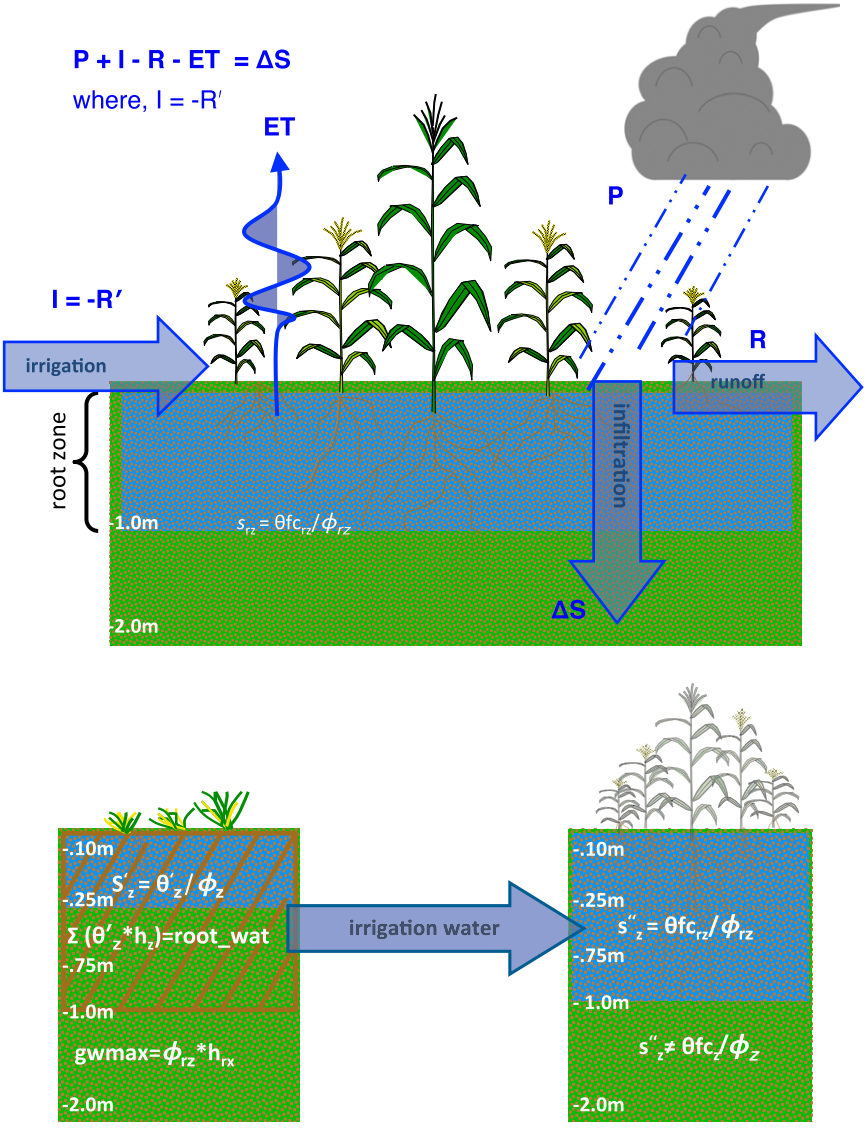

FIG. 1. (top) Schematic showing the principle components of the irrigation scheme in RegCM3-IBIS, where P is precipitation, ET is evapotranspiration, R is runoff, I is irrigated water supplied, S is storage, s_{rz} is the relative soil saturation in the root zone (1 m), $\theta_{fc_{rz}}$ is the root zone's volumetric soil moisture at field capacity, and ϕ_{rz} is the root zone porosity. (bottom) Schematic illustrating the important soil depths and soil moisture/water values needed to transition from a dry soil to an irrigated soil column. Note that z is the reference value of each specific soil layer depth in the column (0.10, 0.25, 0.75, 1.00, and 2.00 m), and h is the depth of each of the soil layers (0.10, 0.15, 0.50, 0.25, and 1.00 m).

5) If frac_wat is less than rel_fc, then irrigated water is required and the amount of water needed to bring to the relative field capacity is calculated (wat_req):

$$\text{wat\_req} = \text{root\_wat} - (\text{rel\_fc})(\text{gwmax}). \quad (5)$$

6) Add water relative to each soil layer's depth h_z/h_{rz} to update the relative soil saturation from s' to s'' for each layer:

$$s'' = \left[\frac{(h_z/h_{rz})(-\text{wat\_req})}{h_z\phi_z}\right] + s'. \quad (6)$$

7) Add wat_req as (negative) runoff:

$$R = R + \text{wat\_req}. \quad (7)$$

8) Repeat for each time step (or scheduling time step).

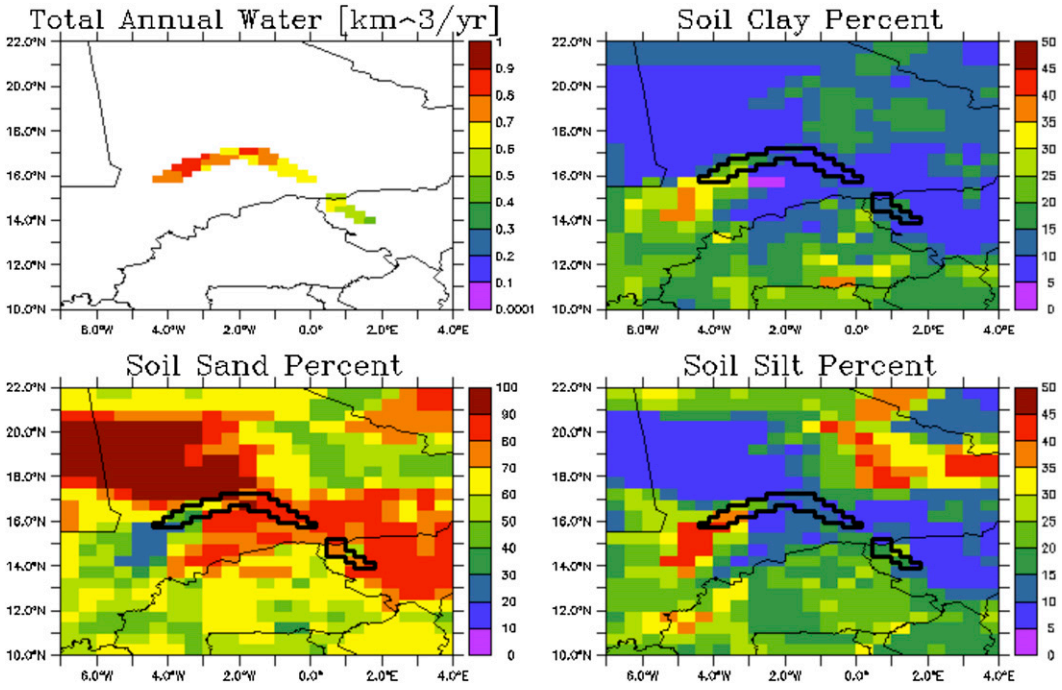

FIG. 2. Total annual water ($km^3\,yr^{-1}$) required to irrigate each grid cell and the soil texture types (percent clay, sand, and silt) over the region. Note that the black outlined areas represent those that are irrigated cropland in the irrigation experiment.

It is important to note that the scheme does not result in each layer's soil moisture being at that layer's actual relative field capacity. Rather, the entire root zone is at the root zone's weighted average relative field capacity. As a result, this difference causes relative soil saturation values of the top two layers to be larger than the bottom two layers, which has higher relative field capacities than the top layers, as more water is now applied in the top two soil layers. This assumption is more consistent with flood irrigation where water is applied to the surface.

In addition to land constraints, irrigation is limited by the actual flow of the Niger River. Figure 2 quantifies the total annual water required by the irrigation scheme for each grid cell as well as highlighting the effect of soil texture and climate on the water requirements. With each 30 km × 30 km grid cell requiring between 0.5 and 0.8 $km^3\,yr^{-1}$, the total water needed to irrigate over this region is 21 $km^3\,yr^{-1}$; this value is significantly less than the total annual flow of the Niger River (approximately 70 $km^3\,yr^{-1}$). Moreover, it can be seen in the farther north region, which is drier, that more water needs to be supplied. In addition, the amount of water required is largely a function of the soil texture. That is, in regions with higher clay and silt values, the water requirements are larger. The larger water requirements are a direct result of clay and silt having larger field capacities. With larger values, these texture types can hold more water and therefore the soil moisture values at field capacity are larger.

3. Experimental design

A 30-yr simulation of RegCM3-IBIS, centered at 14°N, 3°E and 30-km resolution, with 180 points in the zonal and 200 points in the meridional direction using a Mercator projection is performed over West Africa. The first year of simulation is used as model spinup and therefore not used in analysis. The domain covers most of West Africa from the Mediterranean Sea in the north to the Congo and Atlantic Ocean in the south. Figure 3 represents the model domain and vegetation biomes. The prescribed vegetation biomes are taken from the potential natural vegetation dataset of Foley et al. (1996) with cropland added from the work of Ramankutty and Foley (1998); the simulation is performed in static vegetation mode, meaning biomes are not allowed to evolve over time. The Grell scheme is chosen to model moist convection within RegCM3-IBIS with the Fritsch and Chappell closure employed (Grell et al. 1994). All other physics packages used in these simulations are of the standard configuration of RegCM3-IBIS. Pal et al. (2007) offers a comprehensive overview and description of RegCM3 and its capabilities. The dynamic vegetation model (IBIS) adds several layers of

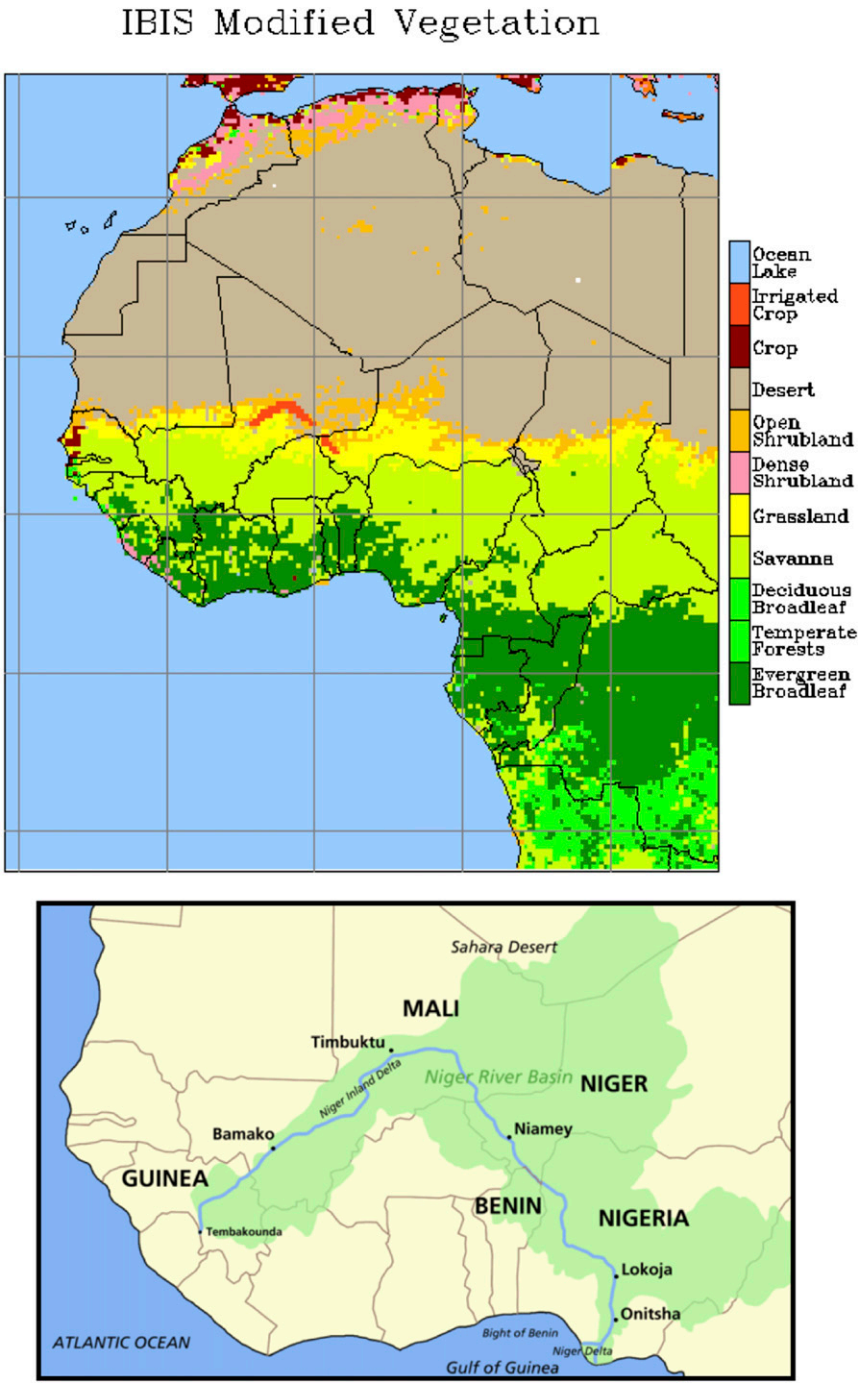

FIG. 3. (top) RegCM3-IBIS modified vegetation domain implemented for ICONT, reflecting altered land cover (to irrigated cropland, red-orange grid cells) for ICONT over the Niger River basin region of Mali and Niger. (bottom) Map showing the Niger River and its basin. The river begins in the wet highlands of Guinea before traversing northward to the dry Sahel in Mali and Niger before bending back southward, reaching its outlet in the Gulf of Guinea in Nigeria.

increased sophistication when compared to other land surface models, such as Biosphere–Atmosphere Transfer Scheme (BATS) of Dickinson et al. (1986). To begin with the model includes six soil layers down 2 m from the surface as well as representations for soil biogeochemistry, vegetation dynamics, and vegetation phenology. The authors refer readers to Winter and Eltahir (2010) for a more detailed model description.

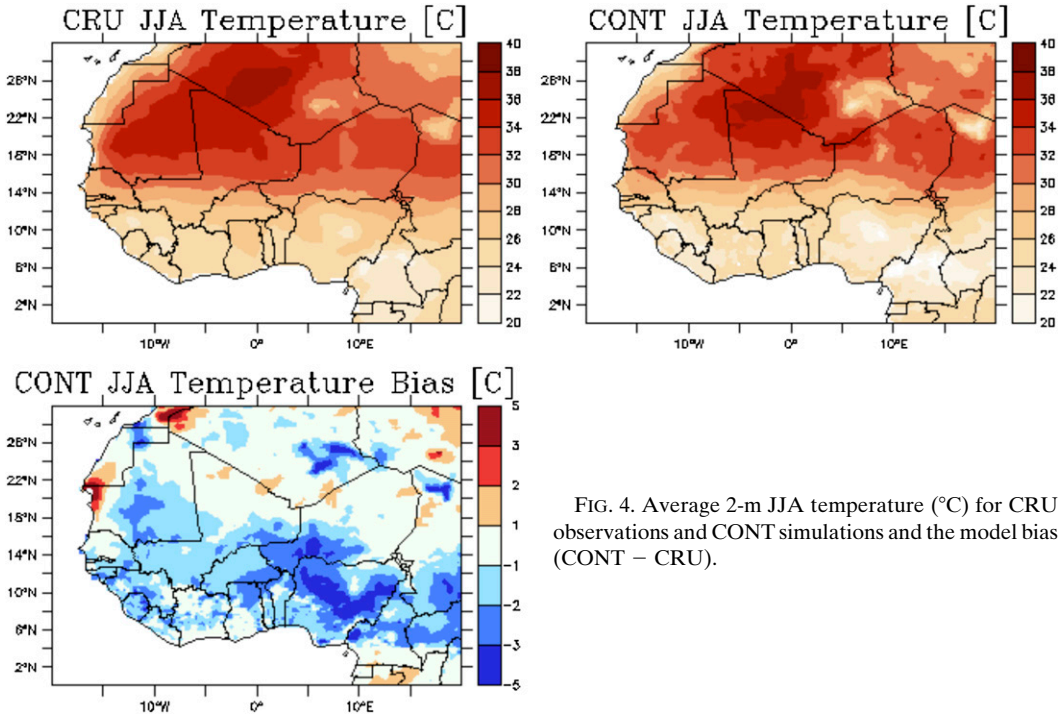

FIG. 4. Average 2-m JJA temperature (°C) for CRU observations and CONT simulations and the model bias (CONT − CRU).

Initial and boundary conditions are implemented from the 40-yr European Centre for Medium-Range Weather Forecasts (ECMWF) Re-Analysis (ERA-40) dataset for the period of 1972–2002 (Uppala et al. 2005). Lateral boundary conditions (LBCs) were forced by applying the sponge relaxation of Perkey and Kreitzberg (1976). SSTs are prescribed to RegCM3 from the Met Office Hadley Centre Global Ice Coverage and Sea Surface Temperature (GISST) optimally interpolated dataset (Rayner et al. 2006). The SST datasets are $1° \times 1°$ monthly resolution and are based on in situ and satellite observations. This simulation will be hereafter referred to as CONT.

According to a 1997 Food and Agriculture Organization of the United Nations (FAO) report analyzing irrigation potential in Africa, nearly 30 000 km^2 of land in the Niger River basin can be irrigated (see Fig. 3). Based on the arable land over the region of Mali and Niger, a RegCM3 simulation is completed where 33 grid cells (approximately 29 700 km^2) are altered to irrigated cropland. This region is located along the bend of the Niger River in the countries of Mali and Niger (shown in Fig. 3). A 30-yr simulation is performed where the open shrubland, grasses, and desert grid cells of the upper Niger River in Mali and Niger are converted to irrigated cropland (Fig. 3). Other than the irrigated croplands, the domain setup and configuration is identical to CONT and will be hereafter referred to as ICONT.

4. Performance of baseline model to observations

In efforts to show that RegCM3-IBIS can accurately model most of the surface features that will be examined in this work, presented below are results from the control's (no irrigation) 30-yr simulation compared to observations. First, surface (2 m) temperature and precipitation are presented and compared to seasonal observations in latitude–longitude plots using the Climate Research Unit (CRU)'s interpolated gridded datasets for surface monthly temperature and precipitation (Mitchell and Jones 2005). Then, zonally averaged, monthly model results are measured against a suite of different observational datasets for temperature, precipitation, shortwave and longwave radiation, and humidity.

a. Summer average daily temperature

Shown in Fig. 4 is boreal summer [June–August (JJA)], seasonally averaged 2-m temperatures for CRU observations and the CONT simulation. As seen in Fig. 4, RegCM3 does well in simulating the JJA reverse meridional temperature gradient, with maximum temperatures close to 40°C found in northern Mali and the Sahara Desert in both observations and model output. Conversely, by the Gulf of Guinea, local minimum temperatures of about 22°C are both present in CRU and CONT. As a result, temperatures are within 2°C

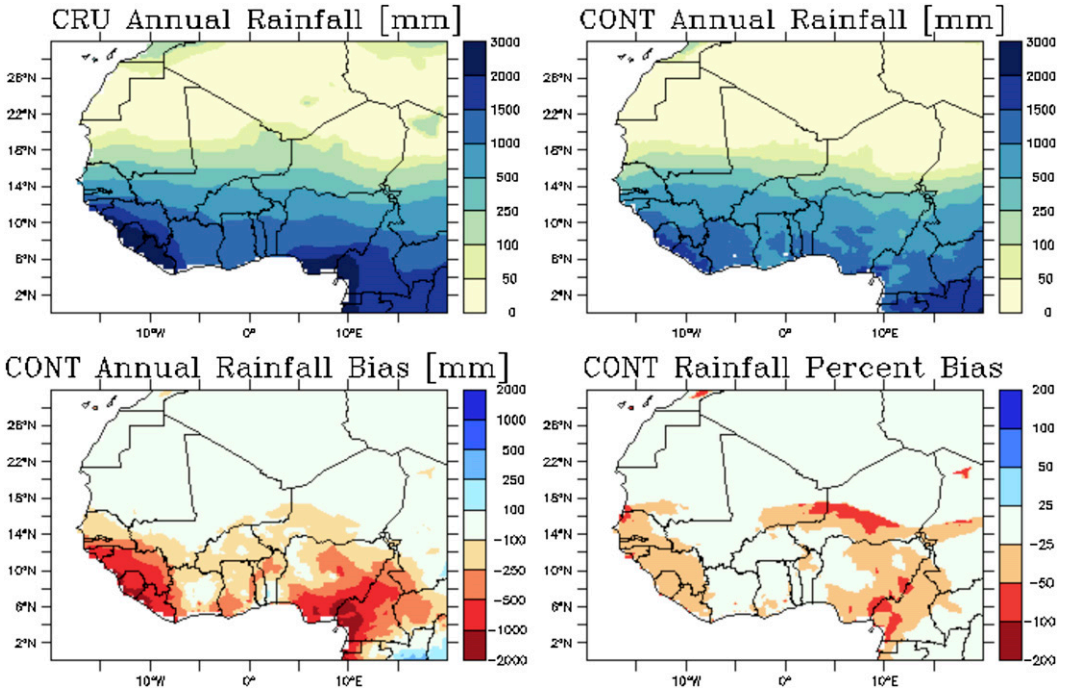

FIG. 5. Average annual rainfall (mm) for CRU observations and CONT simulations and the model bias (CONT − CRU) and percent bias.

throughout most of the domain and therefore within an acceptable range. Most importantly across our region of interest in central Mali and southern Niger, the bias is within 1°–2°C.

b. Annual and monsoon season rainfall

Next, an examination of simulated rainfall totals is completed at the annual time scale and for the peak of the monsoon season [June–September (JJAS)] (Figs. 5 and 6). RegCM3 does well in capturing the tight rainfall gradient across the Sahel region with yearly simulated rainfall less than 50 mm in northern Mali and Niger, yet nearly 1 m in the southern portions of both countries (see Fig. 5). Moreover, CONT sufficiently models the wet region of the Gulf of Guinea with rainfall totals close to observations of 2 m. However, RegCM3 exhibits a strong dry bias by Guinea, Sierra Leone, and the Ivory Coast. Similarly, in the eastern portion of the domain, a pronounced dry bias occurs across Cameroon and the Congo region. Both features are well documented in many regional climate model (RCM) simulations over the region (Druyan et al. 2010). Both areas have strong topographical gradients that are not completely captured at 30-km resolution. As a result, it is believed that orographic lifting and the resulting enhanced rainfall is not sufficiently modeled. In any event, overall annual rainfall biases are within 25% of observations across most of the Sahara, Sahel, and Gulf of Guinea.

Similarly, RegCM3-IBIS sufficiently simulates the monsoon peak (JJAS) rainfall totals over most of West Africa (see Fig. 6). More specifically, across much of the Sahel, CONT satisfactorily captures the 50–500-mm gradient of rainfall from central Mali and south to Burkina Faso—in the region where our experiments include irrigation. Moreover, present in the annual rainfall as well, a noticeable dry bias across the coastal mountain regions of Guinea and Cameroon is plainly seen, with annual rainfall on the order of 500 mm. Since these two locations receive nearly 2 m of rainfall during this time of the year, the bias is about 35% across these highlands. Overall, it is shown that RegCM3-IBIS is able to reproduce adequately both spatial patterns as well as magnitudes of West African rainfall and temperature.

5. Performance of irrigation scheme

Further analysis on the monthly time scale is carried out for a grid cell (centered at 16.5°N, 3°W) that is modified from an open shrubland to an irrigated cropland (Fig. 7). With irrigation beginning in May and ending in September, the figure shows that supplied water ranges from 3 to 8 mm day^{-1} depending on the month. Early in the season (May), when the ground is dry, the irrigation scheme must add the most water to bring the soil moisture level to field capacity. After this initial supply, the amount of water needed to maintain

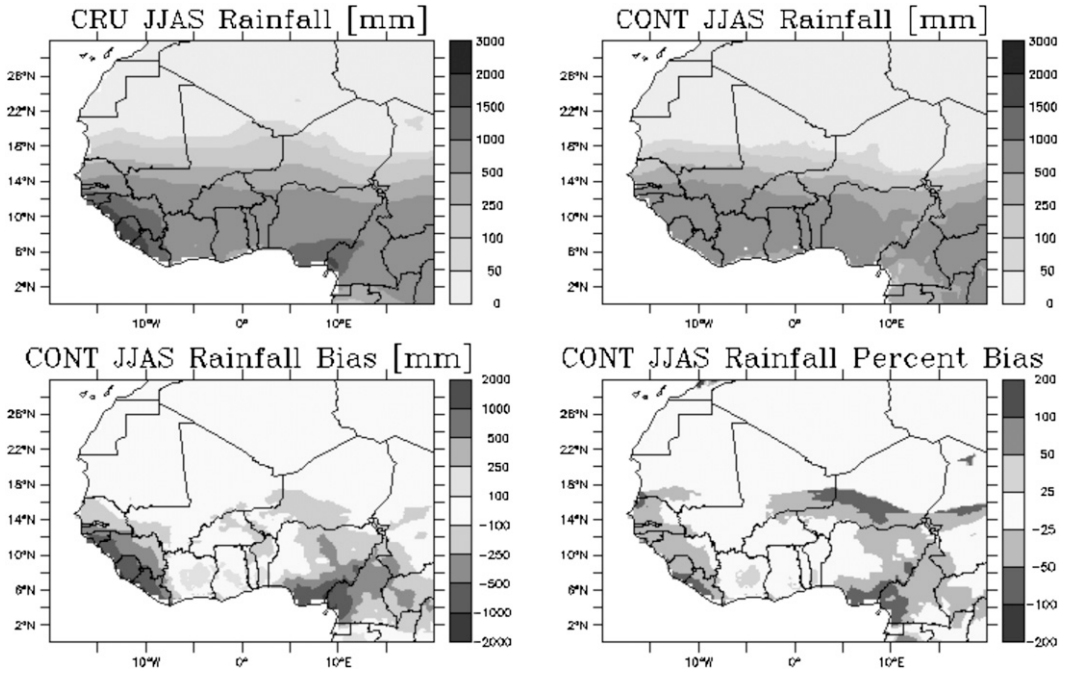

FIG. 6. As in Fig. 5, but for the monsoon peak season (JJAS).

this soil moisture value decreases as the monsoon rainfall progresses farther northward. By August, the amount of irrigation reaches its minimum at about 3 mm day^{-1}, corresponding with the maximum rainfall rates of 2 mm day^{-1}. Another clear feature from Fig. 7 is the effect of dry and wet years on the water supply for irrigation. For example, 1987 represents a dry year over this grid cell and hence significantly more water is required via irrigation. Conversely, the following year is relatively wet as the monsoon reaches the region earlier in the season and is somewhat stronger. Thus, the average July, August, and September water applied in

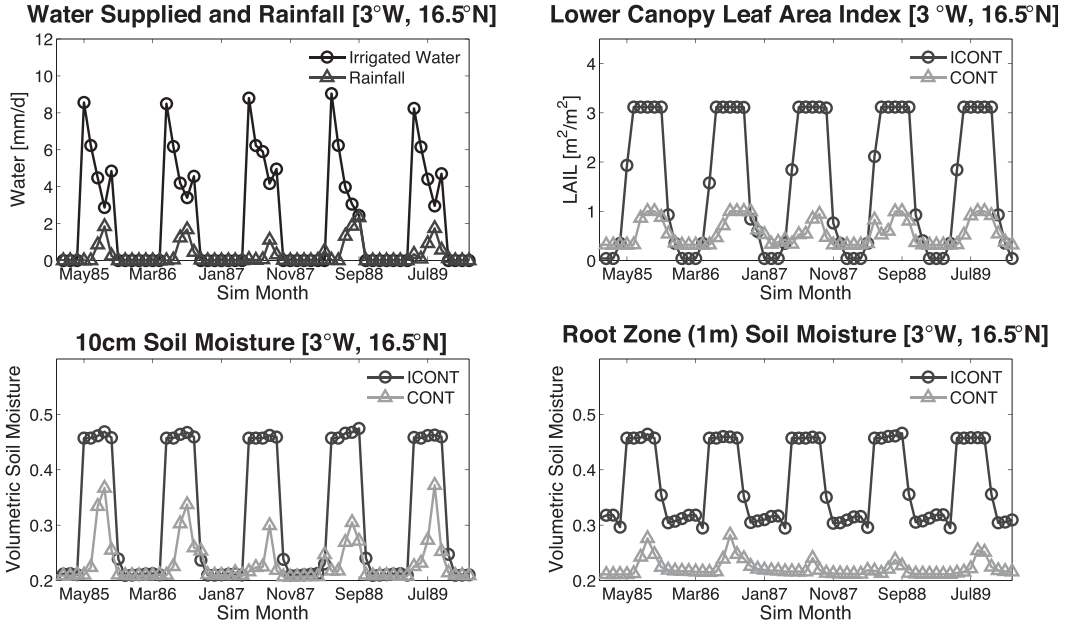

FIG. 7. Monthly point analysis (16.5°N, 3°W) of a grid cell that transitions from a shrubland (CONT) to an irrigated cropland (ICONT) for the simulated years of 1985–90. Shown are the irrigated water supplied (mm day^{-1}), rainfall (mm day^{-1}), LAIL (m^2 m^{-2}), and relative soil saturation for the top and root zone layers in both CONT and ICONT.

1988 is only 3 mm day^{-1}, where in 1987 the value is closer to 5 mm day^{-1}; therefore, the amount of irrigation required can vary by more than 150 mm during the season, depending on the climatic conditions.

Given ample water from May to September, it is expected that significant plant growth, or greening, would occur over the shrubland turned irrigated field during these summer months. This result is observed when examining the lower canopy leaf area index (LAIL) over the grid cell in ICONT versus CONT (Fig. 7). The LAIL, a direct measure of the leaf area of a crop, shrub, or grass, is a good proxy for plant growth and vegetation cover in the lower vegetation canopy and will be used as an indicator of greening (increase in LAIL) in model simulations. With copious sunlight and sufficient water the LAIL of ICONT reaches nearly 3 times the value of CONT (3.1 versus 1.1 m^2 m^{-2}). Succinctly, crops grow with plentiful water, while shrubs and grasses struggle in the dry conditions. Also noticeable is the crop's delayed onset or growing period, as maximum LAIL occurs in June even though irrigation begins in May. Likewise, the maximum LAIL continues through October even though irrigation has ceased. By November, the crop begins to die off as the soil moisture greatly decreases and the LAIL drops to zero. Unlike the cropland, the shrubland LAIL (CONT) is strongly dependent on the monsoon rains of JJAS and responds as such. Although the shrubs and grasses never reach the height and coverage of the crop, it is interesting to note that in the dry season, the LAIL of CONT is larger than ICONT (0.3 versus 0.0). Where the crop PFT is quite water sensitive and ceases to live in the dry months, the shrubs and grasses are able to adapt to lower soil moisture and thus persist, in some capacity, during the winter and spring seasons.

Furthermore, Fig. 7 shows the effects of irrigation on the soil moisture of the top soil layer (first 10 cm) and the root zone (top 1 m). Where CONT's soil moisture exhibits seasonality based on the monsoon, ICONT's soil moisture is a function of the irrigation scheduling—from May to September—and it responds as quickly as the water is applied (i.e., at 0.46 in May). However, the top 10 cm sometimes does breach the relative field capacity during the rainy season as the soil becomes saturated at the surface; this is not experienced, however, throughout the root zone layer. By October, the soils dry rather quickly and values match closely to CONT's. Nevertheless, the increase in relative soil saturation ranges from 50% to 150% with the most dramatic changes, as expected, in the drier, tail months of May and September. These results imply a strong sensitivity of plant growth to soil moisture values. That is, for a 50% increase in soil moisture, a nearly twofold increase in LAIL can occur. As a result, it is clear that the region is largely water limited for plant development.

Figure 8 further illustrates the performance of IBIS's irrigation scheme by highlighting differences between ICONT and CONT simulations for JJA surface features affected by irrigation: soil moisture, vegetative fraction, lower canopy leaf area index, and plant canopy height. As expected, the irrigated fields have relative soil saturation values ranging from 0.2 to 0.4, larger than the control; this increase is nearly a doubling of the soil moisture over the region. The largest increases occur across the drier northern portions of the crop land in Mali. With increased available water, plant coverage dramatically expands across the Mali irrigated fields with some regions seeing a 75% increase in vegetative fraction (see Fig. 8). Following suit, the LAIL across the irrigation is significantly larger in ICONT and CONT. Interestingly, the irrigated fields of Niger do no exhibit such a large change in soil moisture, vegetative fraction, or LAIL. These results are due to the irrigated region in Niger already being fairly wet during the JJA season as RegCM3-IBIS simulates the monsoon progressing this far north as well as relative field capacity values smaller over this sandy area. Finally, the resulting increase in canopy height is a further indication of the greening effect of irrigation as the Mali crop lands exhibit a 0.5–1.0-m increase in the lower canopy height. Such results not only help confirm that the irrigation scheme of RegCM3-IBIS works properly, but also that irrigation over this region could significantly alter the landscape and the surrounding environment of the Niger River delta.

6. Effects on West African climate

As seen in Fig. 3, the scale irrigation coverage is quite small compared to the overall size of the domain: 33 grid cells versus 36 000 total grid cells, which is less than a 1% change in the domain's land cover. Therefore, analysis focuses on local, surrounding climate change effects. The discussion that follows details the effects on the local surface energy, hydrology, and climate features caused by irrigation of the upper Niger. Analysis is kept to boreal summer (JJA; Table 1) as irrigation only occurs two months outside of this period (May and September). Likewise, during these months the monsoon rarely reaches these regions. Thus, when examining September through May, little change was found in any of the climatic fields.

a. Surface energy fluxes and hydrologic cycle

Figure 9 shows the effects of irrigation on the summertime daily 2-m temperatures. When including irrigation,

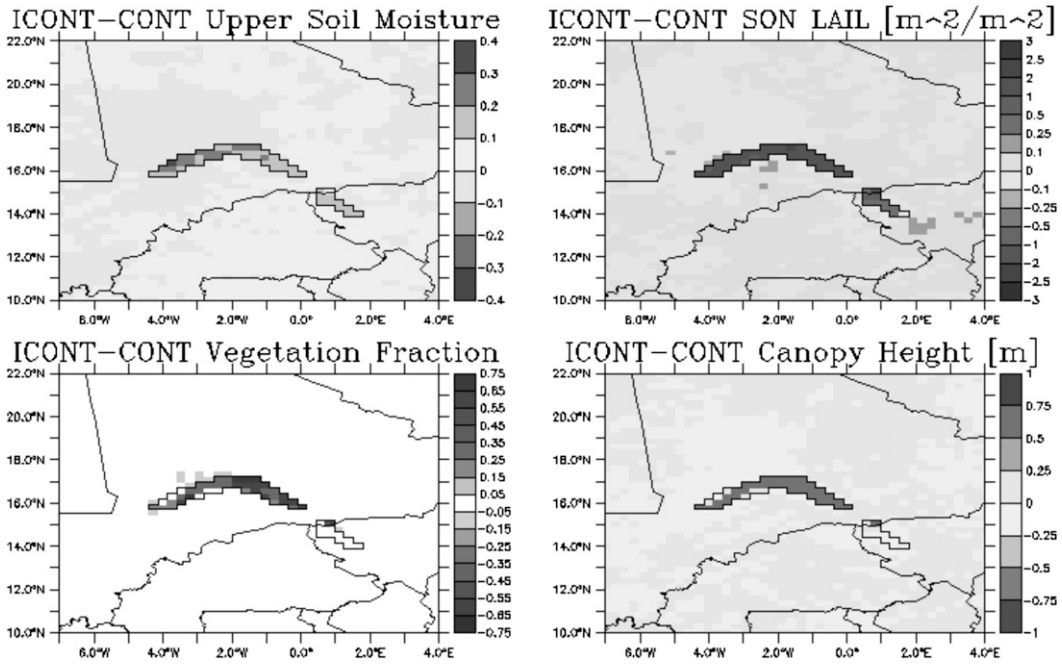

FIG. 8. Differences between ICONT and CONT's JJA upper-layer soil moisture, vegetation fractional coverage, LAIL ($m^2\,m^{-2}$), and canopy height (m), highlighting the effects of irrigation on surface features. Note that the outlined grid cells represent those that are irrigated in ICONT.

the resulting drop in daily temperature over the irrigated croplands is quite dramatic; an average cooling of nearly 5°C occurs throughout all the irrigated grid cells. However, the temperature decrease is not just felt in the irrigated fields. Seen in Fig. 9 is the 0.5°–1°C daily cooling that occurs to the north and east of the irrigated fields in Mali and Niger. With prevailing southwesterly winds, advection of the cooler air over the irrigated fields occurs across this region.

Introduction of irrigation results in a darkening of surface albedo, a cooling of surface temperatures, and an increase in moisture in the atmosphere. With a darker surface, the absorbed shortwave radiation increases across the irrigation. In contrast, the outgoing net longwave radiation decreases as temperature cooling reduces upward longwave radiation and additional water vapor increases downward longwave radiation. Thus, the resulting net radiation over the irrigated fields increases 25–70 $W\,m^{-2}$. These changes lead to a decrease in the sensible heat flux by 40–80 $W\,m^{-2}$ (Fig. 9). However, to compensate for the additional net radiation and the reduction in sensible heat, the latent heat flux largely increases over the irrigated croplands by 65–150 $W\,m^{-2}$ (see Fig. 9).

Examining the change in evaporation and transpiration in the increased ET field indicates that additional transpiration via crops contributes more than increased evaporation (not shown). Evapotranspiration increases nearly 2–4 mm day^{-1} from May through September with nearly 2–3 mm day^{-1} attributed to increased transpiration. Without irrigation, the partitioning between evaporation and transpiration is nearly equal. These results are consistent with significantly larger LAIL values in ICONT than CONT. Interestingly, the largest increase in evaporation (~1 mm day^{-1}) occurs early in the irrigation season—May through June; while crops are still growing, some of the additionally supplied water can evaporate from the bare ground soil.

An increase in evapotranspiration, as expected, leads to an increase in the surface specific humidity over the irrigated region (Fig. 10). The moistening over the

TABLE 1. Summary of JJA average daily temperature (TA), specific humidity (QA), rainfall (PRE), latent heat (LH), sensible heat (SH), PBL height, and moist static energy (MSE) in CONT and ICONT simulations for the period of 1973–87 over all irrigated cropland grid cells. Also shown is the difference between the two simulations.

	CONT	ICONT	ICONT − CONT
TA (°C)	31.5	27.3	−4.2
QA ($g\,kg^{-1}$)	12.1	16.5	4.4
PRE (mm $month^{-1}$)	36	30	−6
LH ($W\,m^{-2}$)	31	146	115
SH ($W\,m^{-2}$)	79	8	−71
PBL height (m)	1027	486	−541
MSE ($kJ\,kg^{-1}$)	335	341	6

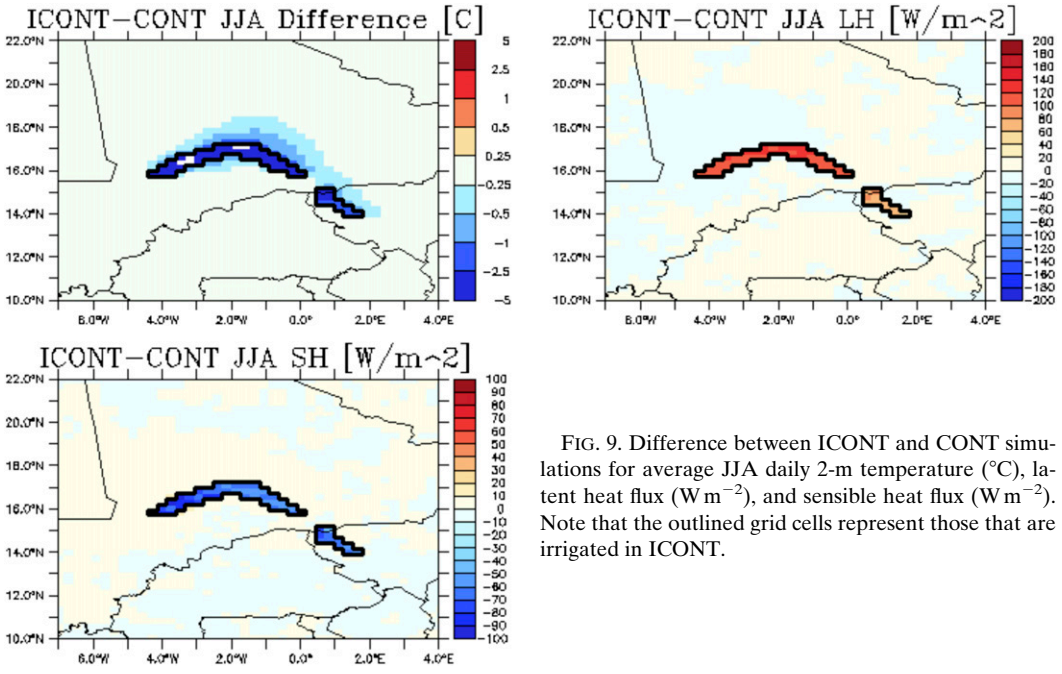

FIG. 9. Difference between ICONT and CONT simulations for average JJA daily 2-m temperature (°C), latent heat flux ($W\,m^{-2}$), and sensible heat flux ($W\,m^{-2}$). Note that the outlined grid cells represent those that are irrigated in ICONT.

irrigated region is quite substantial with values increasing on average from 13 to 18 $g\,kg^{-1}$. The change in the southern irrigated field (in Niger) is quite less (1–2 $g\,kg^{-1}$); this region is already quite humid and wetter than the region farther north. However, as seen with the temperature, the more humid air is not just experienced over the irrigation. Farther north and to the east of the fields, daily specific humidity values increase by 0.5–1 $g\,kg^{-1}$. As seen in Fig. 10, the percent change of such an increase is not significantly large (less than 10%), but the change in relative humidity is significant in some of those regions (Fig. 10). Surface daily relative humidity across the irrigated fields increases by over 30% as cooler temperatures combined with more water vapor results in values as high as 80%–90% across western Mali. Just outside the irrigated area, the advection of cooler and more humid air does cause the range in relative humidity values to rise from 40%–45% to 50%–55%. The increase in boundary layer relative humidity and moist static energy should result in an increase in the convective efficiency and hence rainfall totals.

Therefore, the difference between annual rainfall for the two simulations is presented in Fig. 11. As can be seen, the overall magnitude and spatial distribution of rainfall over the region remains largely unchanged. However, it is clearly seen that rainfall over the irrigated land itself decreases. For example, across the western and southern portion of the irrigation in Mali, annual rainfall totals decrease by 50–100 mm; that is nearly a 25%–50% reduction in the annual rainfall (Fig. 11). The change across central and western Mali is statistically significant at the 95% confidence level when using the Welch's *t* test. Seasonal changes in rainfall indicate that 90% of this drying occurs during JJA when most rainfall occurs over the Sahel (not shown). As alluded to earlier, no change in rainfall occurs in either December–February (DJF) or March–May (MAM). These results are expected since this period is the region's dry season and irrigation does not occur during this timeframe either. In September, slight decreases (on the order of 10%–20%) in rainfall just to the west of the Mali crop fields occur, but the overall maximum is less than 20 mm.

The decrease in rainfall here is not a result of decreased convective efficiency but rather a decrease in the triggering of convection (i.e., a reduction in the number of convective events). Therefore, the increase in convective efficiency due to higher relative humidity and moist static energy is dwarfed by the decrease in convective triggering from a strong collapsing of the boundary layer height. These phenomena can be seen when examining changes in the planetary boundary layer (PBL) height (Fig. 11). Large reductions in the surface temperature and the sensible heat flux reduce the average daily boundary layer height by more than 700 m, a 50% reduction of the total height. Therefore, the PBL does not grow enough to trigger convection. Essentially, the irrigation causes the lower atmosphere to be too cool for moist convection to occur over the

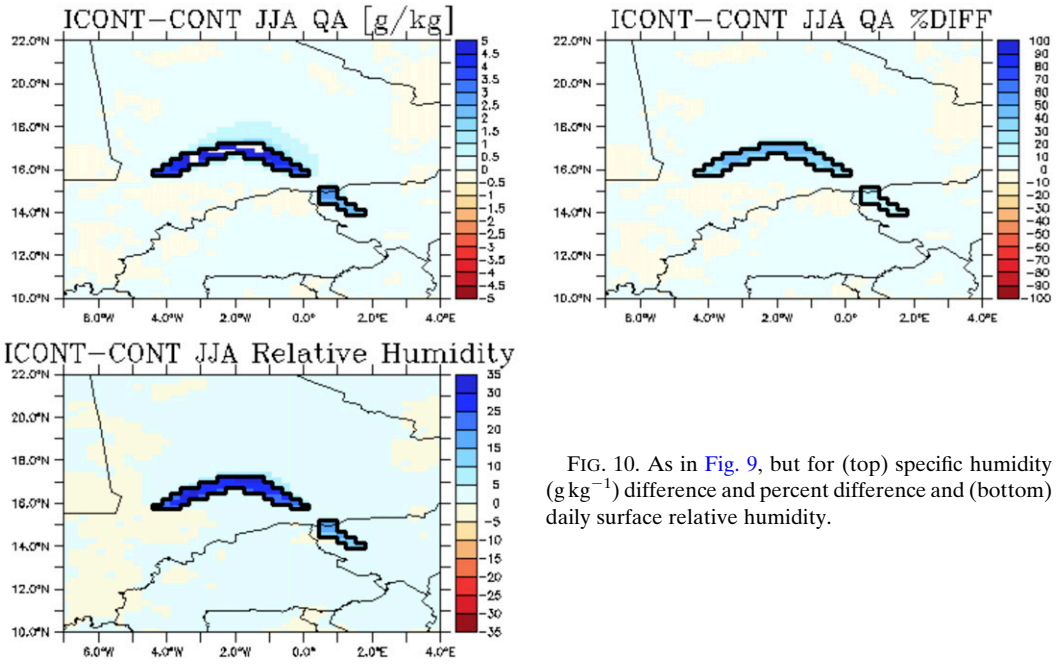

FIG. 10. As in Fig. 9, but for (top) specific humidity ($g\,kg^{-1}$) difference and percent difference and (bottom) daily surface relative humidity.

irrigated fields. As a result, the convective inhibition, or the negative buoyant energy needed to overcome for free ascent of an air parcel is never breached and convection occurs less often. These phenomena are illustrated in Fig. 12, where the number of days with moist convection (i.e., convective rainfall over 1 mm) is plotted. Clearly evident is the large reduction of days with moist convection as ICONT receives 5–15 days less of convective rainfall than the control simulation. This reduction results in approximately a 20%–40% decrease in total days per year of convective triggering and spatially matches well with the rainfall differences of

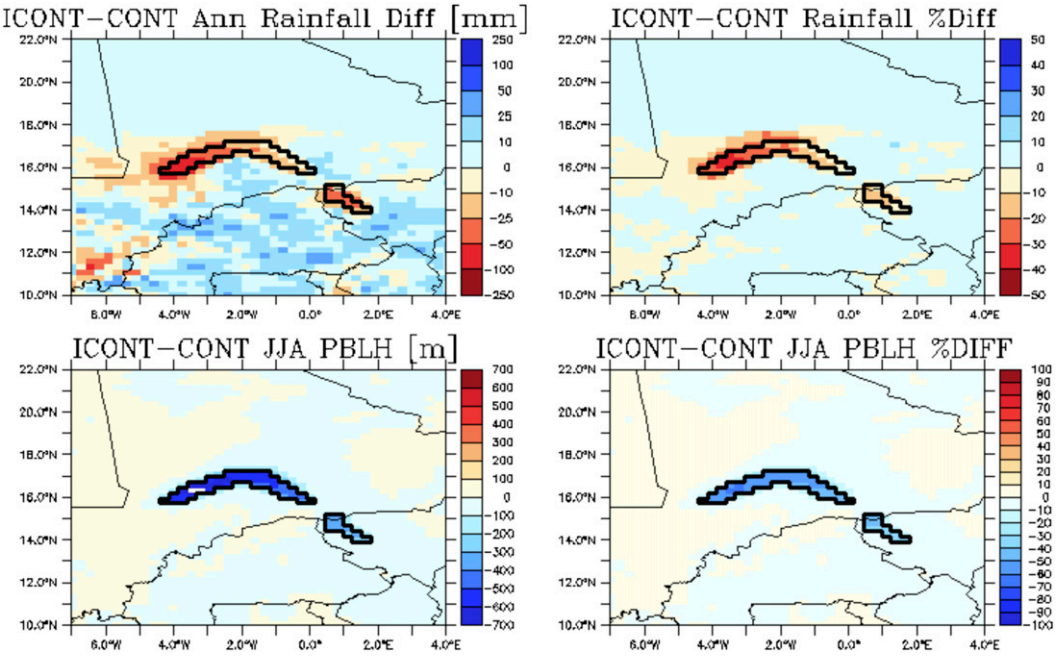

FIG. 11. As in Fig. 9, but for (top left) annual rainfall ($mm\,yr^{-1}$) and (bottom left) PBL height (m). (right) Percent differences between ICONT and CONT for the two values.

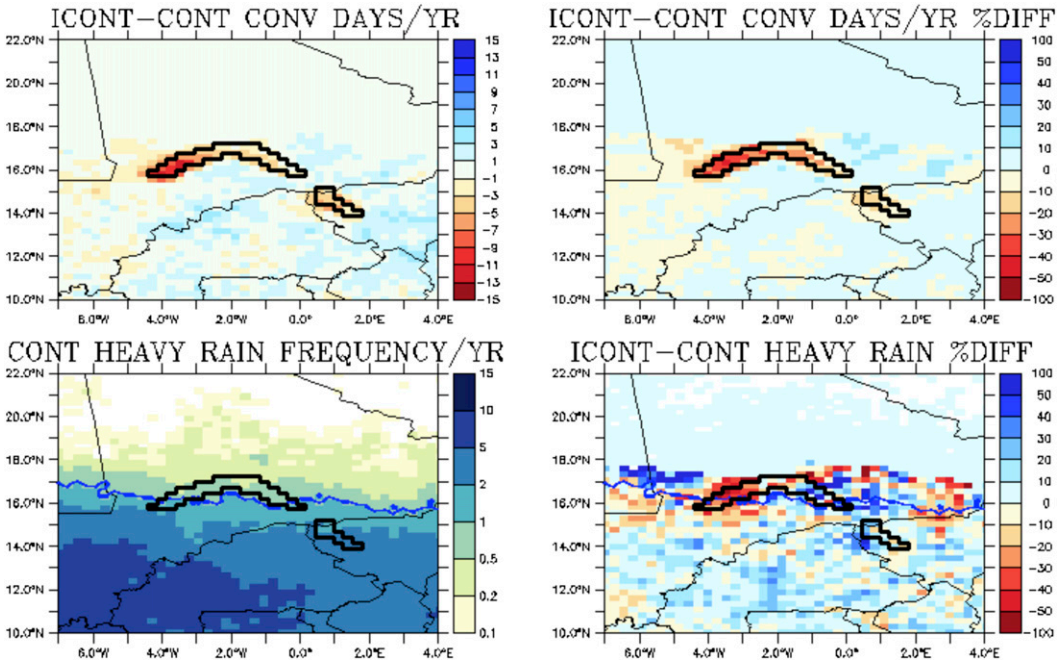

FIG. 12. (top) Difference and percent difference of days with moist convection (convective rainfall greater than 1 mm day^{-1}) per year between ICONT and CONT. (bottom) Frequency of heavy rainfall events (12.7 mm day^{-1} or more) in CONT and the percent difference of heavy events between ICONT and CONT. Note that the outlined grid cells represent irrigation in ICONT, and the blue contour in the bottom panels delineates the one event per year frequency value.

Fig. 11. Finally, Fig. 12 shows the frequency of heavy rainfall events across the region, where heavy rainfall is defined as 12.5 mm day^{-1}. As expected, there is a tight gradient in the frequency of these events as one moves south across the region. Over the irrigated fields of Mali, the frequency of such an event is 0.5–1.0 or once every other year or once a year. Interestingly, the irrigation seems to have a larger effect on these heavier rainfall events as a nearly 50% reduction occurs in heavy rainfall events over the irrigated cropland. Therefore, less convective triggering of these strong, wetter storms largely accounts for the decrease in total rainfall. This result further illustrates that irrigation affects convective triggering more so than convective efficiency.

To confirm this mechanism, a simulation is performed where irrigation only occurs in the first week of each month from May through September. Results indicated a warmer (by 1.0°–1.5°C), drier irrigated region in which the boundary layer decreases on average 250 m less than that in ICONT. As a result, convection was triggered 48% of the time (days in JJA) over the area as opposed to 32% in ICONT (note that CONT has convection triggered 50% of the time). As a result, rainfall values were higher over the crop fields in west Mali when compared to ICONT. Therefore, we are able to confirm that the drastic cooling and collapsing of the boundary layer can account for the drier irrigated fields of west Mali in the ICONT simulation.

b. *Vertical profiles of atmospheric variables*

With substantial changes in temperature and humidity at the surface, analysis of the change in vertical profiles of atmospheric fields is completed for 1500 UTC (also 1500 local time) across the irrigated region. Figure 13 reveals that perturbations made to the land surface do not penetrate significantly aloft as vertically plotted differences (latitudinally averaged) are computed. For example, temperature cooling is only experienced to about 850 mb (1 mb = 1 hPa), with a sharp drop-off in the signal aloft. However, as seen at the surface, the temperature reduction does extend vertically to the east of the actual irrigated region. Likewise, the increase in humidity is strongly constrained to the lowest 100 mb (Fig. 13). Drying aloft in the midatmosphere (500–700 mb) is consistent with less convection and vertical transport of moisture, as seen with the reduction of rainfall over the western portion of the cropland. Given intense surface cooling and significantly reduced boundary layer heights, the increased moisture and decreased temperature is largely constrained to the surface and lower atmosphere. As a result, any change in moist static energy, albeit large (1–3 kJ kg^{-1} increase), is also

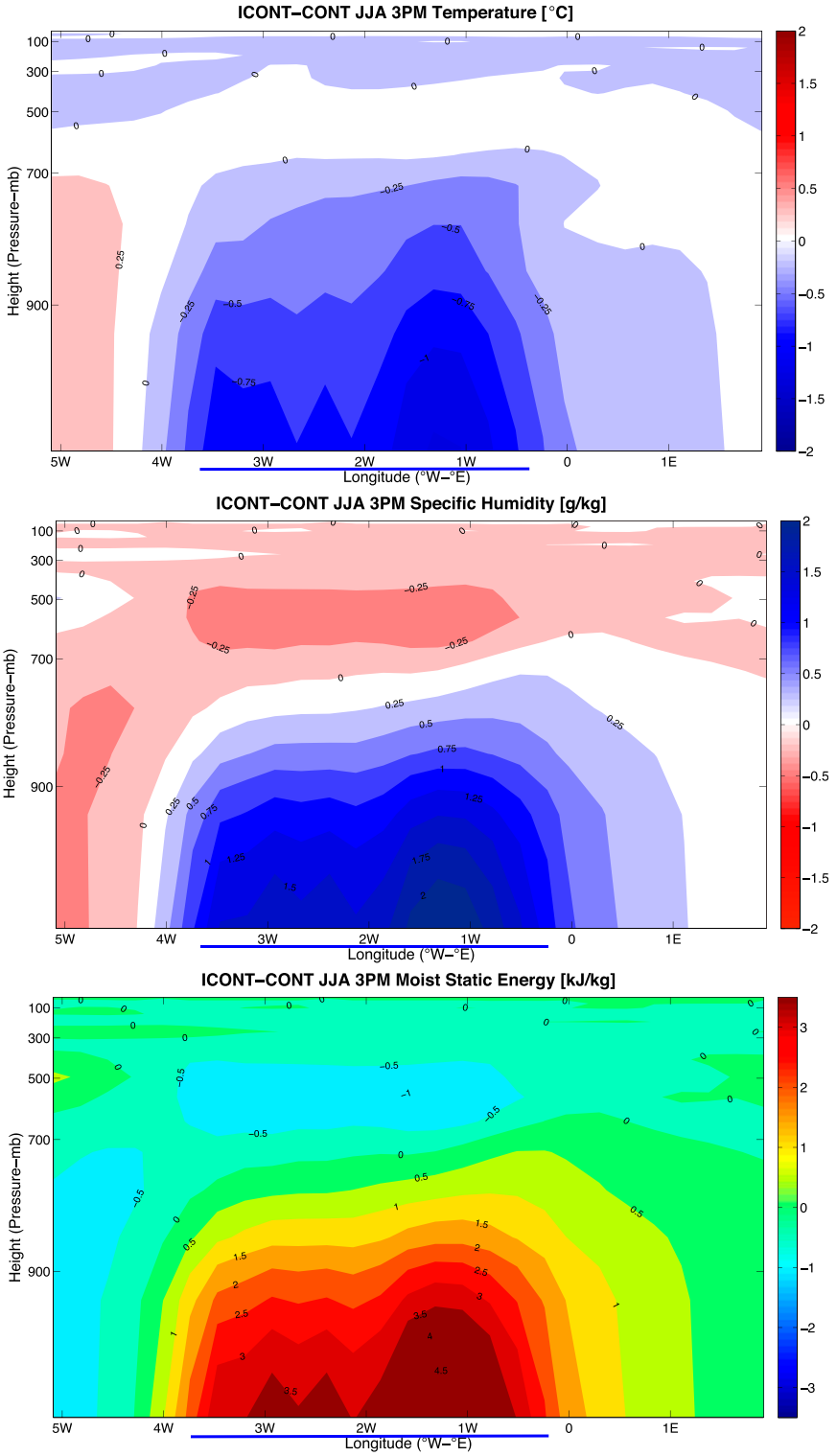

FIG. 13. Vertical profiles of longitudinal cross-section differences (averaged from 16° to 17.5°N) between ICONT and CONT average JJA 1500 UTC for (top) temperature (°C), (middle) specific humidity (g kg^{-1}), and (bottom) moist static energy (kJ kg^{-1}) with a logarithmic height scale. The blue line underneath each x axis represents the zonal extent of the irrigated cropland.

contained close to the surface (i.e., in only the lowest 100 mb of the atmosphere) and thus not experienced by the surrounding atmosphere or aloft.

7. Conclusions and future work

This work presents and highlights the performance of a new scheme added to RegCM3-IBIS for irrigation croplands. The new vegetation biome is populated with a crop plant functional type that can exclusively exist in an irrigated grid cell. Likewise, an irrigated cropland grid cell is supplied water to the root zone until it reaches relative field capacity. Moreover, the new scheme allows for irrigation scheduling, that is, when water is to be applied to the system. Initial results show a large sensitivity of the scheme to soil texture types, how the water is applied, and the climatic conditions over the region. The new irrigation scheme is tested over West Africa, specifically in the countries of Mali and Niger where a realistic representation of irrigation of the Niger River is performed by constraining the land irrigated by the annual flow of the Niger River and the amount of arable land in the region as reported by the FAO (Frenken and Faures 1997).

Over West Africa, a 30-yr simulation including irrigation is compared to an identical simulation that does not include irrigation of the Niger River. Results show significant greening of the irrigated land as evapotranspiration over the area largely increases, namely, via increases in transpiration from plant growth resulting from increased soil moisture. The increase in the evapotranspiration, or latent heat flux, causes a significant decrease in the sensible heat flux with surface temperatures cooling on average by nearly 5°C. This cooling is felt downwind where temperatures outside the irrigation are reduced by 0.5°–1.0°C. Likewise, large increases in specific humidity are experienced across the irrigated cropland (on the order of $5\,g\,kg^{-1}$), but also extend farther north and east, reflecting the prevailing surface southwesterlies.

Furthermore, it is concluded that in the scheme's current state (i.e., irrigation at every time step), the module significantly overestimates realistic water supply practices for irrigation. Much research has examined the most effective and realistic approach to supplying water to an irrigation scheme (Kanamaru and Kanamitsu 2008; Sorooshian et al. 2012). These studies also find that in most saturated or relative field saturated schemes, excessive cooling and evapotranspiration occurs. Here, we performed an experiment where irrigation is scheduled only for the first week of each month. The model demonstrated a large sensitivity to this technique as temperature cooling and moistening were significantly reduced and hence improved. Future work further examining different irrigation scheduling techniques would be useful in addressing known cool biases caused by the representation of irrigation in land surface models.

In addition, despite increases in surface relative humidity and moist static energy over the croplands, rainfall decreases over the irrigated lands. The decrease in rainfall can be explained by the large surface cooling and collapse of the boundary layer. With significantly lower boundary layer heights, the triggering of convection is largely hampered as the convective inhibition, or negative buoyant energy is never breached. Outside of the irrigation, no significant change in rainfall occurs. These results can be explained by the lack of change in vertical profiles of atmospheric quantities with irrigation. That is, although humidity and moist static energy values increase greatly at the surface, these changes do not extend further than the lowest 50–100 mb of the atmosphere during the afternoon. Therefore, the atmosphere is more or less disconnected from the surface changes, most likely due to the large reduction in the boundary layer height.

Given a new anthropogenic biome in IBIS, several opportunities present themselves for future study. To begin with, the use of different crop types and scheduling techniques should be examined across West Africa and other regions across the globe for sensitivity analysis of crop water demand and effect on local climates. That is, different crops, and their associated phenology, would respond differently in certain climate zones and therefore may alter the cropland's effect on local climate. Likewise, adding a harvesting and land clearing module to irrigated croplands would be effective in making the scheme more realistic. Finally, this work concludes that there is not a strong connection between the land surface and the atmosphere as perturbations caused by irrigation leave insignificant effects aloft. However it is important to note that this lack of signal may be a result of the irrigated region being comparatively small to the overall domain and subregion. Thus, it would be necessary to perform additional experiments with larger regions covered with irrigated lands. Nevertheless, future studies should examine how the convection scheme and land surface model are coupled dynamically. More succinctly, the sensitivity of a convection scheme to land surface perturbations should be fully investigated.

Acknowledgments. The authors are very grateful to all members of the Eltahir group and MIT Parsons Laboratory that contributed in some way to this work. In particular, we are especially thankful to Jonathan Winter, who without his technical assistance and valuable

insight, this work would not be possible. This work has been funded through support by the Kuwait Foundation for the Advancement of Science.

REFERENCES

Adegoke, J., R. Pielke, J. Eastman, R. Mahmood, and K. Hubbard, 2003: Impact of irrigation on midsummer surface fluxes and temperature under dry synoptic conditions: A regional atmospheric study of the U.S. High Plains. *Mon. Wea. Rev.,* **131,** 556–564, doi:10.1175/1520-0493(2003)131<0556:IOIOMS>2.0.CO;2.

Dickinson, R., P. Kennedy, A. Henderson-Sellers, and M. Wilson, 1986: Biosphere-Atmosphere Transfer Scheme (BATS). NCAR Tech. Note NCAR/TN-275+STR, 69 pp., doi:10.5065/D6668B58.

Druyan, L., and Coauthors, 2010: The WAMME regional model intercomparison study. *Climate Dyn.,* **35,** 175–192, doi:10.1007/s00382-009-0676-7.

Foley, J., I. Prentice, N. Ramankutty, S. Levis, D. Pollard, S. Sitch, and A. Haxeltine, 1996: An integrated biosphere model of land surface processes, terrestrial carbon balance, and vegetation dynamics. *Global Biogeochem. Cycles,* **10,** 603–628, doi:10.1029/96GB02692.

Frenken, K., and J.-M. Faures, 1997: Irrigation potential in Africa: A basin approach. FAO Land and Water Bull. 4, 177 pp. [Available online at http://www.fao.org/docrep/W4347E/W4347E00.htm.]

Grell, G. A., J. Dudhia, and D. Stauffer, 1994: A description of the fifth-generation Penn State/NCAR Mesoscale Model (MM5). NCAR Tech. Note NCAR/TN-398+STR, 121 pp.

Haddeland, I., D. Lettenmaier, and T. Skaugen, 2006: Effects of irrigation on water and energy balances of the Colorado and Mekong River basins. *J. Hydrol.,* **324,** 210–223, doi:10.1016/j.jhydrol.2005.09.028.

Kanamaru, H., and M. Kanamitsu, 2008: Model diagnosis of nighttime minimum temperature warming during summer due to irrigation in the California Central Valley. *J. Hydrometeor.,* **9,** 1061–1072, doi:10.1175/2008JHM967.1.

Kucharik, C. J., and Coauthors, 2000: Testing the performance of a dynamic global ecosystem model: Water balance, carbon balance, and vegetation structure. *Global Biogeochem. Cycles,* **14,** 795–826, doi:10.1029/1999GB001138.

Kueppers, L., M. Snyder, and L. Sloan, 2007: Irrigation cooling effect: Regional climate forcing by land-use change. *Geophys. Res. Lett.,* **34,** L03703, doi:10.1029/2006GL028679.

Lobell, D., G. Bala, A. Mrin, T. Phillips, R. Maxwell, and D. Rotman, 2009: Regional differences in the influence of irrigation on climate. *J. Climate,* **22,** 2248–2255, doi:10.1175/2008JCLI2703.1.

Marcella, M. P., and E. A. B. Eltahir, 2012: Modeling the summertime climate of Southwest Asia: The role of land surface processes in shaping the climate of semiarid regions. *J. Climate,* **25,** 704–719, doi:10.1175/2011JCLI4080.1.

Mitchell, T. D., and P. D. J. Jones, 2005: An improved method of constructing a database of monthly climate observations and associated high-resolution grids. *Int. J. Climatol.,* **25,** 693–712, doi:10.1002/joc.1181.

Pal, J., and Coauthors, 2007: Regional climate modeling for the developing world: The ICTP RegCNET and RegCM. *Bull. Amer. Meteor. Soc.,* **88,** 1395–1409, doi:10.1175/BAMS-88-9-1395.

Perkey, D. J., and C. W. Kreitzberg, 1976: A time-dependent lateral boundary scheme for limited-area primitive equation models. *Mon. Wea. Rev.,* **104,** 744–755, doi:10.1175/1520-0493(1976)104<0744:ATDLBS>2.0.CO;2.

Pielke, R. A., Sr., J. O. Adegoke, T. N. Chase, C. H. Marshall, T. Mastui, and D. Niyogi, 2007: A new paradigm for assessing the role of agriculture in the climate system and in climate change. *Agric. Meteor.,* **142,** 234–254, doi:10.1016/j.agrformet.2006.06.012.

Ramankutty, N., and J. Foley, 1998: Characterizing patterns of global land use: An analysis of global croplands data. *Global Biogeochem. Cycles,* **12,** 667–685, doi:10.1029/98GB02512.

Rayner, N., D. Parker, E. Horton, C. Folland, L. Alexander, D. Rowell, E. Kent, and A. Kaplan, cited 2006: Met Office's Global Ice Coverage and Sea Surface Temperatures (GISST), and monthly night marine air temperature/SST anomalies (MOHMATN4)/(MOHSST6) data (1856-2006). [Available online at http://badc.nerc.ac.uk/view/badc.nerc.ac.uk__ATOM__dataent_GISST.]

Segal, M., Z. Pan, R. Turner, and E. Takle, 1998: On the potential impact of irrigated areas in North America on summer rainfall caused by large-scale systems. *J. Appl. Meteor.,* **37,** 325–331, doi:10.1175/1520-0450-37.3.325.

Sorooshian, S., J. Li, K. Hsu, and X. Gao, 2012: Influence of irrigation schemes used in regional climate models on evapotranspiration estimation: Results and comparative studies from California's Central Valley agricultural regions. *J. Geophys. Res.,* **117,** D06107, doi:10.1029/2011JD016978.

Uppala, S., and Coauthors, 2005: The ERA-40 Re-Analysis. *Quart. J. Roy. Meteor. Soc.,* **131,** 2961–3012, doi:10.1256/qj.04.176.

Winter, J. M., and E. A. B. Eltahir, 2010: The sensitivity of latent heat flux to changes in the radiative forcing: A framework for comparing models and observations. *J. Climate,* **23,** 2345–2356, doi:10.1175/2009JCLI3158.1.